Published in final edited form as:
Nanotoxicology. 2011 December ; 5: 531–545. doi:10.3109/17435390.2010.530004.

Mast cells contribute to altered vascular reactivity and ischemia-reperfusion injury following cerium oxide nanoparticle instillation

CHRISTOPHER J. WINGARD[1], **DIANNE M. WALTERS**[1], **BROOK L. CATHEY**[1], **SUSANA C. HILDERBRAND**[2], **PRANITA KATWA**[2], **SIJIE LIN**[3], **PU CHUN KE**[4], **RAMAKRISHNA PODILA**[4], **APPARAO RAO**[4], **ROBERT M. LUST**[1], and **JARED M. BROWN**[2]

[1]Department of Physiology, Brody School of Medicine, East Carolina University, Greenville, North Carolina

[2]Department of Pharmacology and Toxicology, Brody School of Medicine, East Carolina University, Greenville, North Carolina

[3]California NanoSystems Institute, University of California Los Angeles, Los Angeles, California

[4]Department of Physics and Astronomy, Clemson University, Clemson, South Carolina, USA

Abstract

Cerium oxide (CeO_2) represents an important nanomaterial with wide ranging applications. However, little is known regarding how CeO_2 exposure may influence pulmonary or systemic inflammation. Furthermore, how mast cells would influence inflammatory responses to a nanoparticle exposure is unknown. We thus compared pulmonary and cardiovascular responses between C57BL/6 and B6.Cg-*Kit*$^{W\text{-}sh}$ mast cell deficient mice following CeO_2 nanoparticle instillation. C57BL/6 mice instilled with CeO_2 exhibited mild pulmonary inflammation. However, B6.Cg-*Kit*$^{W\text{-}sh}$ mice did not display a similar degree of inflammation following CeO_2 instillation. Moreover, C57BL/6 mice instilled with CeO_2 exhibited altered aortic vascular responses to adenosine and an increase in myocardial ischemia/reperfusion injury which was absent in B6.Cg-*Kit*$^{W\text{-}sh}$ mice. *In vitro* CeO_2 exposure resulted in increased production of PGD_2, TNF-α, IL-6 and osteopontin by cultured mast cells. These findings demonstrate that CeO_2 nanoparticles activate mast cells contributing to pulmonary inflammation, impairment of vascular relaxation and exacerbation of myocardial ischemia/reperfusion injury.

Keywords

Mast cell; mast cell deficient mice; osteopontin; sash mice; ischemia-reperfusion injury

Correspondence: Dr Jared M. Brown, PhD, Department of Pharmacology and Toxicology, Brody School of Medicine, East Carolina University, Medical Sciences Building, 6W-33 600 Moye Blvd, Greenville, NC 27834. Tel: +1 252 744 2108. Fax: +1 252 744 3203. brownja@ecu.edu.

Declaration of interest: This work was supported by National Institute of Environmental Health Sciences (NIEHS) RO1ES016246 (CJW) and NIH RO1ES019311 (JMB). The authors declare they have no competing financial interests. The authors report no conflict of interest. The authors alone are responsible for the content and writing of the paper.

Introduction

Cerium oxide (CeO_2) represents an important nanomaterial with a wide range of applications such as solar cells, fuel cells, gas sensors, oxygen pumps, and use as a fuel additive (Health Effects Institute 2001). In addition, CeO_2 has been proposed for medical use due to its reported antioxidant capabilities and is currently listed as one of five nanomaterials under investigation by the U.S. Environmental Protection Agency (Niu et al. 2007; Colon et al. 2009). However, few studies have examined its inflammatory effects both *in vitro* and *in vivo*, and in particular, how CeO_2 may impact systemic inflammatory responses.

Tissue mast cells, which have been traditionally studied in the context of allergic disease, are now well documented to play a role in innate and acquired immune responses. Similarly, they contribute to tissue repair and maintenance of homeostasis (Brown et al. 2008) and control of vascular reactivity through endothelial-dependent and independent processes (Doyle et al. 1994; Dileepan and Stechschulte 2006). In addition to these studies, we have reported that mast cells are activated by crystalline silica particles and that mast cell deficient mice (B6.Cg-*Kit*$^{W\text{-}sh}$) exposed to silica do not develop silicosis while wild-type mice develop extensive pulmonary inflammation and fibrosis (Brown et al. 2007). Because of these many functions of mast cells, and in a time when nanomaterials such as CeO_2 are being proposed for therapeutic use and present potential environmental exposure risks, it is of interest to understand how mast cells may respond to these unique materials.

In the current study, we utilize a pulmonary instillation of CeO_2 nanoparticles to investigate the cardiovascular inflammatory responses to a particle exposure and the role mast cells may have in this process. Thus, we entered into experiments testing the hypothesis that mast cells influence the cardiovascular response to CeO_2 exposure *in vivo* and verified *in vitro* that CeO_2 can direct mast cell activation. As will be shown, mice with a normal population of mast cells (C57BL/6) exhibited mild pulmonary inflammation, but had greater effects on aortic vascular responses and myocardial ischemia/reperfusion injury following instillation of CeO_2. In contrast, mast cell deficient B6.Cg-*Kit*$^{W\text{-}sh}$ mice instilled with CeO_2 did not exhibit similar effects on both pulmonary and cardiovascular endpoints. Lastly, as will be shown, CeO_2 directed mast cell production of pro-inflammatory mediators *in vitro*.

Materials and methods

Mice

Mast cell deficient (B6.Cg-*Kit*$^{W\text{-}sh}$/HNihrJaeBsmJ) and wild-type (C57BL/6J) mice were obtained from Jackson Laboratories at 4–6 weeks of age (Bar Harbor, ME, USA). Mast cell deficiency in the B6.Cg-*Kit*$^{W\text{-}sh}$ mice occurs through a transversion mutation in the receptor c-kit (Grimbaldeston et al. 2005; Wolters et al. 2005). Therefore, mast cells, which require stem cell factor (the ligand for c-kit) for proliferation and maturation, do not develop in these mice. In addition to reports confirming lack of mast cells in these mice, we have determined that lung sections from 4- to 6-week old mice do not contain mast cells as determined by toluidine blue staining (data not shown) (Grimbaldeston et al. 2005; Wolters et al. 2005). Only male mice were used throughout this study and the two strains were matched by age and body weight. The average weight of the C57BL/6 mice was 26.1 g and 24.7 g for the B6. Cg-*Kit*$^{W\text{-}sh}$ mice and were used at approximately 8 weeks of age. Mice were anesthetized with isofluorane before oropharyngeal instillation of either 100 μl sterile saline or 100 μl sterile saline suspension of 10, 30 or 100 μg CeO_2 particles. Oropharyngeal instillation was performed with the tongue gently held in full extension and the suspension was pipetted on to the base of the tongue, this technique provides for a wide dissemination of particle in a peribronchiolar pattern within the lung parenchyma (Rao et al. 2003). Six to

eight mice of each strain were instilled per group, and the groups consisted of C57BL/6J or B6.Cg-*Kit*$^{W\text{-}sh}$ mice receiving either saline or CeO_2 instillations. Mice were sacrificed 24 h post-instillation. All animal procedures were performed in accordance with the National Institutes of Health guidelines and approved by the East Carolina University institutional animal care and use committee. All animals were treated humanely and with regard for alleviation of suffering.

CeO_2 particles and characterization

CeO_2 nanoparticles obtained from Melorium Technologies (Rochester, NY, USA) are reported by the manufacturer to have an average particle size of 8 nm and surface area of 44 m^2/g. To characterize the CeO_2 nanomaterial in our laboratories, we dispersed the particles in a saline solution at 1 μg/μl and the mixture was bath-sonicated (1510R-MTH, Branson Ultrasonics Corp.) for 45 min to obtain a suspension. The hydrodynamic size distribution of the CeO_2 suspension was characterized using dynamic light scattering (Malvern Instruments, Nanosizer S90). The surface charge of the CeO_2 suspension was measured using a zeta potential device (Malvern Instruments, Zeta ZS). The size and aggregation of the CeO_2 suspension was determined using a transmission electron microscope (TEM) (Hitachi 7600). Specifically, a total volume of 50 μl CeO_2 suspension (1 μg/μl) was pipetted onto a 200-mesh copper grid and dried at room temperature for 1 h prior to imaging. Osmium tetroxide counter staining was omitted to the samples in order to eliminate the introduction of precipitation artifacts. The TEM images were acquired at a high voltage of 120 kV. Micro-Raman spectra of CeO_2 nanoparticles within mouse lung sections were obtained in a Horiba Jobin-Yvon Dilor XY triple grating spectrometer equipped with an Olympus IC 100 optical microscope using Argon ion laser excitations at 514.5 nm. For mapping purposes, sterile pyrex slides containing lung sections from mice instilled with CeO_2 nanoparticles were placed on an automated stage operated in steps of 0.1 microns.

Cell culture and CeO_2 treatment

Mouse BMMCs were cultured from femoral marrow cells of C57BL/6 mice. Cells were cultured in RPMI 1640 supplemented with 10% FBS, 100 U/ml penicillin, 100 μg/ml streptomycin, 25 mM HEPES, 1 mM sodium pyruvate, nonessential amino acids (Sigma-Aldrich, St. Louis, MO, USA), 0.0035% 2-mercaptoethanol, and 300 ng/ml recombinant murine IL-3 (PeproTech, Rocky Hill, NJ, USA). BMMCs were used after 4–6 weeks of culture, a time at which > 95% of cells are mast cells as determined by expression of the high affinity IgE receptor (FcεRI). Cells were treated with CeO_2 in 96-well plates at 0, 10, 30, and 100 μg/ml. Cell viability was determined by lactate dehydrogenase (LDH) release. The percentage of LDH release was measured in supernatants of BMMCs exposed to CeO_2 for 24 h (BioVision, Mountain View, CA, USA). Untreated cells were used as a negative control and 1% Triton X-100 treated BMMCs were used as a positive control, representing 100% LDH release.

In vitro BMMC degranulation and cytokine release

For degranulation experiments, BMMCs were seeded at 5×10^4 cells/well in a 96-well plate and sensitized overnight with 100 ng/ml mouse IgE anti-DNP (Sigma-Aldrich). For treated samples, CeO_2 was added for 24 h before addition of 100 ng/ml DNP-HSA (Sigma-Aldrich). After 30 min incubation with DNP-HSA at 37°C, *p*-nitrophenyl-*N*-acetyl-β-D-glucopyranoside was added to cell supernatants and lysates (generated by addition of 0.1% Triton-X-100) for 90 min as a chromogenic substrate for *N*-acetyl-β-D-hexosaminidase. The reaction was stopped with 0.2 M glycine. Optical density was measured at 405 nm using a Synergy HT microplate reader (BioTek, Winooski, VT, USA). β-Hexosaminidase release was expressed as the percentage of total cell content after subtracting background release from unstimulated cells. Mouse osteopontin was measured in cell culture supernatants of

BMMCs seeded at 2×10^5 cells/well 24 h after addition CeO_2 using a mouse Duo-Set ELISA system (R&D Systems, Minneapolis, MN, USA). Mouse PGD_2 was measured 1 h after addition of CeO_2 using a mouse EIA system (Cayman Chemical, Ann Arbor, MI, USA). In addition, the cytokines TNF-α, osteopontin and TGF-β (R&D Systems) were measured in non-infarcted heart tissue. Heart tissue was extracted and homogenized in a modified RIPA buffer (Tallboys Engineering Corp. Montrose, PA, USA). Protein was quantified using an EZQ Protein Quantification Kit (Molecular Probes, Inc. Eugene, OR, USA). Samples were normalized based on the heart homogenate with the lowest protein concentration. Values are reported for heart tissue as pg/μg of total protein.

Quantitative Real-Time PCR

Total RNA from BMMCs or heart tissue was isolated using Qiagen RNeasy Mini Kit (Qiagen, Valencia, CA, USA). RNA was reverse transcribed using a QuantiTect reverse transcription kit (Qiagen). Quantitative real-time PCR was performed using QuantiTect primer assays and SYBR green master mix (Qiagen). A Bio-Rad iCycler was used to obtain cycle threshold (Ct) values for target and internal reference cDNA levels. Target cDNA levels were normalized to GAPDH, an internal reference using the equation $2^{-[\Delta Ct]}$, where ΔCt is defined as $Ct_{target} - Ct_{internal\ reference}$. Values shown are the average of four independent experiments.

Bronchoalveolar lavage and cell differential

The right lung of saline and CeO_2-instilled mice was lavaged *in situ* four times with Hanks balanced salt solution (HBSS). Brochoalveolar lavage fluid (BALF) was centrifuged at 500 *g* for 10 min at 4°C. Total cells from BALF were counted and an aliquot of 20,000 cells was centrifuged (Cytospin III, Shandon Scientific Ltd, Cheshire, UK) and stained with a three-step hematology stain (Richard Allan Scientific, Kalamazoo, MI, USA). Cell differential counts were determined by morphology with evaluation of 300 cells per slide. Left lung tissue was extracted and homogenized in a modified RIPA buffer (Tallboys Engineering Corp. Montrose, PA, USA). Protein was quantified using an EZQ Protein Quantification Kit (Molecular Probes, Inc. Eugene, OR, USA). Samples were normalized based on the lung homogenate with the lowest protein concentration and were run on ELISAs for osteopontin, IL-6, MIP-1α, IL-10, IL-13, TNF-α and TGF-β (R&D Systems). Values are reported as pg/μg of total protein.

In vitro measurements of vascular isometric force generation

Aorta isolation and ring force generation and relaxation were carried out as reported (Cozzi et al. 2006). Briefly, the thoracic aorta (arch to bifurcation) was removed 24 h after instillation. Aortas were placed in cold MOPS-buffered physiological saline solution (PSS, mM composition: NaCl, 140.0; KCl, 5.0; $CaCl_2$, 1.6; $MgSO_4$, 1.2; 3-[N-mopholino]-propane sulfonic acid (MOPS), 1.2; D-glucose, 5.6; EDTA, 0.02; pH = 7.4 at 37°C) and blood, connective tissue, and fat were removed from each vessel and used immediately in pharmacological dose-response experiments. Thoracic aortic rings (5 mm) were cut from cleaned vessels, vessel rings were either left intact or the lumen gently rubbed to denude the endothelial cell lining. Rings were mounted isometrically with a resting passive tension of 10 mN in a DMT 610 myograph system (DMT-USA International, Atlanta, GA, USA) and bathed in 37°C PSS bubbled with compressed air.

Rings were stimulated with 109 mM K^+PSS solution (in which Na^+ has been substituted with K^+ in an equal molar fashion) for 10 min to insure tissue viability. The rings were relaxed and then subjected to a 1 μM phenylephrine (PE) stimulation followed by a 1 μM acetylcholine-induced relaxation. A functional endothelial relaxation was considered appropriate if the relaxation was > 60% of the PE-induced force; while denuded rings were

appropriate if relaxation was < 10 % of the PE-induced force. After stimulation, aortic rings were rinsed with PSS until passive force was restored. Cumulative concentration response curves were constructed for the α-adrenergic agonist phenyl-ephrine or β-adrenergic agonist norepinephrine (PE and NE, 0.03 – 30 μM) and the endothelial-dependent relaxation agent acetylcholine (ACh, 0.001–100 μM) in 1 μM PE pre-stimulated aortic rings for 5 min. Responses to adenosine and NO donor, sodium nitroprusside (adenosine or SNP, 0.001–100 μM), were also examined in endothelial denuded pre-stimulated aortic rings. Non-linear regression analysis for individual and mean concentration response curves was performed using a Hill fit analysis. Mean data were analyzed by two-way ANOVA, when the ANOVA manifested a statistical difference; the Student-Newman-Keuls test was applied for comparison to vehicle.

Cardiovascular ischemia-reperfusion (I/R) injury

An established protocol (Cozzi et al. 2006) was used to measure I/R injury. Briefly, 24 h post-instillation, mice were anesthetized with sodium pentobarbital (i.p. 60 mg/kg). Anesthesia was maintained by supplemental injections of sodium pentobarbital (30 mg/kg) and body temperature was maintained at 37°C. A midline tracheotomy was preformed and the animals were intubated and mechanically hyper-ventilated with 100% oxygen at a frequency of 120 strokes/min and 0.2 ml tidal volume. After a 10 min equilibration period, the thorax was opened with a left parasternal incision. The pericardium was removed and the left anterior descending coronary artery (LAD) was ligated using a reversible snare applied 4 mm distal to the origin between the conus arteriosus and the left atrium. Following 20 min occlusion, the ligature was released and the LAD was reperfused for 2 h. The percentage of the left ventricle (LV) at risk for ischemia was determined in a separate group of non-exposed control animals subjected to the I/R procedure where the myocardium at risk was delineated by infusing 1% Evan's blue through the aorta. 50% of the LV was at risk for ischemia. In subsequent experiments, the percentage of the LV at risk for ischemia was calculated by multiplying the average area at risk (AAR), determined as described below, by a factor of 0.5. After Evan's blue staining, hearts from saline and CeO_2 exposed mice were excised and 1 mm thick serial sections were cut from the point of ligation to the apex. Sections were incubated 20 min in 1% 2,3,5-triphenyltetrazolium chloride (TTC) solution to demarcate the infarcted from non-infarcted cardiac tissue. Both sides of all sections were imaged and analyzed by computer planimetry (ImageJ, ver. 1.34s) to determine LV tissue area, AAR, and area of infarct. For each side of each section, the infarct was expressed as a percentage of the AAR. The values for all sections from each heart were averaged.

Statistics

Statistical analysis employed PRISM, version 5 (GraphPad, San Diego, CA) and Sigma Plot (SPSS Inc, Chicago, IL). For *in vitro* studies, differences between untreated and CeO_2 treated BMMCs were assessed using one-way ANOVA with Bonferroni post-test. For *in vivo* studies, differences between groups were compared using Student's *t*-test for unpaired observation or ANOVA with Fishers' test for least significant difference. Non-linear regression analysis for individual concentration response curves was performed using a Hill algorithm in Sigma Plot allowing for an individual geometric 'EC_{50}' value to be calculated. Mean data were analyzed by two-way ANOVA. When the ANOVA manifested a statistical difference, the Student-Newman-Keuls test was applied for comparison to vehicle. All values are reported as mean ± SEM. In all cases a *P* value of less than 0.05 was used to indicate statistical significance between groups.

Results

CeO_2 nanoparticle characterization

Figure 1A indicates the average hydrodynamic size of the CeO_2 suspension was 90 ± 20 nm. Our dynamic light scattering measurement further yielded a reduced size of the CeO_2 suspension of 70 ± 20 nm after centrifugation was applied (6,772g RCF) for 2 min. The CeO_2 suspension displayed a zeta potential of −52.7 mV (Figure 1B), suggesting a very stable colloidal state of the nanomaterial. Consistent with our dynamic light scattering measurement, our TEM imaging revealed a similar size distribution of the CeO_2 centered around 70 nm (Figure 1C).

Micro-Raman spectroscopy is an ideal probe for identifying the nature and distribution of nanostructured materials in plants (Lin et al. 2009) and biological species (Roberts et al. 2007). In this study, we determine the distribution of ceria nanoparticles by obtaining a micro-Raman spectral fingerprint of sectioned mouse samples shown in Figure 2A. The characteristic Raman fingerprint of bulk CeO_2 consisted of a dominant peak at 464 cm^{-1} with a typical line width of ~ 20–30 cm^{-1}. This peak results from the vibrational motion (breathing mode) of O atoms around the Ce cations and is known to downshift in frequency with decreasing nanoparticle size due to phonon confinement (Spanier et al. 2001). As shown in Figure 2B inset, a strong Raman peak is observed at ~ 462 cm^{-1} from the boxed area of a mouse lung sample indicating the presence of nanostructured ceria in the boxed region in Figure 2A. Our ability to record such strong sharp Raman peaks enables us to create a Raman map of CeO_2 instilled mouse lung sections (Figures 2B, 2C). Importantly, Raman spectroscopy facilitates depth profiling (confocal Raman) for detecting the CeO_2 nanoparticles embedded deep inside the tissue sections (thickness ~ 8 μm) that may be not be readily accessible for an in-depth electron microscopy analysis (Figures 2C, 2D). The presence of ceria nanoparticles, both on the surface (Figures 2A and 2B) and in the lung tissue (Figures 2C, 2D), is evident from the observation of Raman peak in the CeO_2 exposed mouse lung sections.

Instillation of CeO_2 in C57BL/6 mice, but not B6.Cg-$Kit^{W\text{-}sh}$ mice, results in mild pulmonary inflammation

To assess the *in vivo* toxicity of CeO_2, we first investigated pulmonary inflammation following exposure to CeO_2 nanoparticles and whether mast cells were involved in this response. As shown in Table I, C57BL/6 mice instilled with 100 μg of CeO_2 displayed a significant increase in total BAL cell count as compared to saline instilled mice. This inflammatory response consisted of an increase in macrophages, neutrophils and lymphocytes within the CeO_2 instilled mice. Instillation of 10 or 30 μg CeO_2 also produced a small, but significant increase in neutrophils and lymphocytes (Table I). In contrast, B6.Cg-$Kit^{W\text{-}sh}$ mice instilled with 100 μg CeO_2 did not display an increase in BAL cell infiltration compared to saline-exposed mice

IL-6, MIP-1α and osteopontin are increased in lungs of C57BL/6 mice instilled with CeO_2, while B6.Cg-KitW-sh mice display increased levels of IL-10 in response to CeO_2

To assess potential mechanisms involved in CeO_2-mediated pulmonary inflammation, we measured osteopontin, IL-6, MIP-1α, IL-10, IL-13, TNF-α and TGF-β in lung tissue homogenates from saline and 100 μg CeO_2 instilled C57BL/6 and B6.Cg-$Kit^{W\text{-}sh}$ mice. As shown in Figure 3A and 3B, protein levels of the pro-inflammatory cytokine IL-6 and chemokine MIP-1α were increased in lung tissue of CeO_2 instilled C57BL/6 mice as compared to saline controls, while we did not observe similar findings in B6.Cg-$Kit^{W\text{-}sh}$ mice instilled with CeO_2. Moreover, an increased protein level of the anti-inflammatory cytokine IL-10 was found in B6.Cg-$Kit^{W\text{-}sh}$ mouse lungs of both saline and CeO_2 instilled

mice as compared to C57BL/6 mice (Figure 3C). Lastly, the level of osteopontin in BALF was increased in CeO_2 instilled C57BL/6 mice, but not B6.Cg-*Kit*$^{W\text{-}sh}$ mice (Figure 3D). We did not detect changes in IL-13, TNF-α or TGF-β within lungs of CeO_2 instilled mice (data not shown).

Effects of CeO_2 on thoracic aortic ring isometric force measurements

To assess if pulmonary exposure to CeO_2 can have detrimental effects on systemic vascular reactivity we examined the isometric force responses of segments of endothelial intact or denuded thoracicaorta. Pulmonary instillation of 10, 30 or 100 μg CeO_2 into C57BL/6 mice did not significantly alter the aorticring responses to the adrenergic agonist phenylephrine (data not shown) but had a modest concentration-dependent effect of reducing calculated EC_{50} values for adenosine, norepinephrine and sodium nitroprusside (Table II). Furthermore, the instillation of 100 μg CeO_2 intoC57BL/6 orB6.Cg-*Kit*$^{W\text{-}sh}$ mice had minimal effect on the magnitude (Figure 4) of vascular aortic rings to the vasoactive agents phenylephrine (data not shown), adenosine, norepinephrine and acetylcholine. However, there was a significant difference in aortic ring responses to adenosine when comparing C57BL/6 and B6.Cg-*Kit*$^{W\text{-}sh}$ mice following 100 μg CeO_2 instillation (Figure 4A, right panel). B6.Cg-*Kit*$^{W\text{-}sh}$ mouse aortas displayed an exaggerated contraction to concentrations of adenosine less than 1 μM. Above 1 μM of adenosine, the relaxation profiles were not different between strains or treatments. The aortic ring response to adenosine shows diminishing CeO_2 dose-dependent relaxation in the C57BL/6 mice when compared to saline control. In contrast to C57BL/6 mice, the aortic ring responses from the B6.Cg-*Kit*$^{W\text{-}sh}$ mice instilled with CeO_2 showed an exaggerated constrictor response (Figure 5).

CeO_2 exposure differentially modulates post I/R infarct size in C57BL/6 and B6.Cg-Kit$^{W\text{-}sh}$ mouse hearts

Instillation with 100 μg CeO_2, but not 10 or 30 μg, produced a small but significant increase in heart infarct size as compared to vehicle control in C57BL/6 mice following an episode of ischemia/reperfusion in the heart (Figure 6). In contrast, infarct sizes were not different between saline and 100 μg CeO_2 exposure in B6.Cg-*Kit*$^{W\text{-}sh}$ mice 24 h post-instillation. The overall size of the infarctions was smaller in the B6.Cg-*Kit*$^{W\text{-}sh}$ mice as compared to C57BL/6 saline controls. Areas at risk were not different between groups (data not shown).

TGF-β is increased in hearts of CeO_2 instilled C57BL/6 mice, but not B6.Cg-Kit$^{W\text{-}sh}$ mice

To assess if the increase in I/R infarct size may be due to pre-existing inflammation as a result of CeO_2 exposure, we examined the same cytokine mRNA profile as performed with the lung tissue (osteopontin, IL-6, MIP-1α, IL-10, IL-13, TNF-α and TGF-β) in non-infarcted heart tissue from CeO_2 instilled C57BL/6 and B6.Cg-*Kit*$^{W\text{-}sh}$ mice. We did not detect significant changes in IL-6, MIP-1α, IL-10, or IL-13 expression (data not shown), however, we observed increased mRNA expression of osteopontin, TNF-α and TGF-β in hearts of CeO_2 instilled C57BL/6 mice as compared to saline controls (Figure 7A). Furthermore, mRNA levels for these three cytokines were significantly elevated as compared to mRNA expression in hearts of B6.Cg-*Kit*$^{W\text{-}sh}$ mice instilled with CeO_2 (Figure 7A). While mRNA levels were elevated in hearts of CeO_2 instilled mice, only osteopontin and TGF-β were detectable at the protein level (Figures 7A, 7B). Osteopontin protein levels were not significantly different between saline or CeO_2 instilled C57BL/6 mice, however, TGF-β was significantly increased in CeO_2 instilled C57BL/6 as compared to saline controls. In contrast, TGF-β was not significantly increased above saline controls in the CeO_2 instilled B6.Cg-*Kit*$^{W\text{-}sh}$ mice.

CeO_2 induces release of PGD_2 and osteopontin from BMMC, but exhibits minimal cytotoxicity and no effect on mast cell degranulation

Since we observed differences in both pulmonary and cardiovascular responses to CeO_2 instillation between C57BL/6 and B6.Cg-*Kit*$^{W\text{-}sh}$ mice, we initiated a series of experiments to determine the effects of CeO_2 on cultured mast cells. Minimal cytotoxicity, as measured by LDH release, was detected in BMMCs exposed to 10, 30, and 100 μg/ml CeO_2 for 24 h (0 μg/ml = 2.3% ± 0.5 vs. 10 μg/ml = 2.4% ± 0.4 vs. 30 μg/ml = 1.8% ± 0.3 vs. 100 μg/ml = 1.6% ± 0.6). CeO_2 was next examined for the ability to alter FcεRI-mediated degranulation of BMMCs. Degranulation (as measured β-hexosaminidase release) represents one mechanism by which CeO_2 could enhance mast cell-mediated inflammation. Pretreatment of BMMCs (sensitized with mouse IgE anti-DNP) with CeO_2 at doses of 10, 30 and 100 μg/ml had minimal effect on β-hexosaminidase release after addition of 100 ng/ml DNP-HSA compared with BMMCs that were not exposed to CeO_2 (DNP-HSA Positive = 44.2% ± 10.1 vs. 10 μg/ml = 40.6% ± 17.9 vs. 30 μg/ml = 41.4% ± 21.2 vs. 100 μg/ml = 36.5% ± 16.8). Additionally, CeO_2 exposure by itself did not induce β-hexosaminidase release from BMMCs (data not shown). However, CeO_2 exposed BMMCs increased mRNA expression of several inflammatory cytokines including IL-6, IL-13, TNF-α, TGF-β and osteopontin (Spp1) (Figure 8A). In addition to mRNA expression of cytokines, CeO_2 induced release of PGD_2 and osteopontin in a concentration-dependent manner as compared to untreated BMMCs (Figures 8B, 8C). CeO_2-exposed BMMCs produced a small, but non-significant, increase in TGF-β protein levels (data not shown).

Discussion and conclusion

A role for mast cells in particle-induced pulmonary inflammation has been suggested (Brown et al. 2007); however, the contribution of mast cell activation in the cardiovascular response to nanoparticle exposure has not been explored. In this study, we demonstrate that C57BL/6 mice exhibit mild pulmonary inflammation, altered aortic vascular reactivity and an increase in myocardial ischemia/reperfusion injury 24 h following CeO_2 instillation which was largely absent in B6.Cg-*Kit*$^{W\text{-}sh}$ mast cell deficient mice. Further *in vitro* experiments confirm that CeO_2 can directly activate mast cells to produce inflammatory cytokines and chemokines. Taken together, these data suggest that mast cell activation may represent an underappreciated inflammatory mechanism in response to a nanoparticle exposure.

The potential adverse health effects of CeO_2 nanoparticles has been suggested (Lin et al. 2006; Thill et al. 2006; Park et al. 2007, 2008a, 2008b; Xia et al. 2008), but mechanisms associated with toxicity of CeO_2 have not been elucidated. CeO_2 is reported to induce oxidative stress in a lung epithelial cell line associated with increased ROS and induction of oxidative stress genes (Park et al. 2008b). A similar study demonstrated that CeO_2 induces oxidative stress resulting in decreased cell viability in human lung cancer cells (Lin et al. 2006). However, in contrast, Xia et al. (2008) reported that while CeO_2 is phagocytosed by BEAS-2B and RAW264.7 cells, CeO_2 does not reduce cell viability or increase oxidative stress. Instead, CeO_2 suppressed ROS production and protected the cells from an exogenous source of oxidative stress. These findings are in agreement with studies indicating that CeO_2 is cardioprotective and protects against radiation pneumonitis in mice (Niu et al. 2007; Colon et al. 2009). Since these results are somewhat controversial, we decided to investigate if an *in vivo* nanoparticle exposure impacts the cardiovascular system and whether that response is mediated through mast cells.

Environmental contaminants, including heavy metals, can enhance FcεRI-mediated mast cell degranulation, a response associated with allergic disease (Walczak-Drzewiecka et al. 2003). Therefore, the ability of CeO_2 to alter FcεRI-mediated degranulation was assessed.

CeO_2 by itself did not directly induce degranulation nor did it enhance FcεRI-mediated degranulation. An alternative probable mechanism for mast cell involvement in inflammation and effects on the cardiovascular system associated with CeO_2 is through alteration of cytokine or chemokine levels. This is supported by evidence in the pulmonary system that mast cells are critical in development of silicosis following exposure to silica particles through the *in vivo* alteration of cytokine levels (Brown et al. 2007). Therefore, the ability of CeO_2 to induce inflammatory cytokines was examined. *In vitro* CeO_2 exposure concentration-dependently increased osteopontin, IL-6, IL-13 and TGF-β. In addition, we measured increased IL-6 and MIP-1α in the lungs of C57BL/6 mice instilled with 100 μg CeO_2, but not in the B6.Cg-*Kit*$^{W\text{-}sh}$ mice. Rather, in B6.Cg-*Kit*$^{W\text{-}sh}$ mouse lungs, we found increased levels of the anti-inflammatory cytokine IL-10. These pro-inflammatory mediators contribute to inflammation through recruitment of inflammatory cells including neutrophils and lymphocytes, both of which were increased in the lungs of CeO_2 exposed C57BL/6 mice.

Osteopontin was the most significantly upregulated mediator produced by BMMCs exposed to CeO_2 *in vitro* and C57BL/6 mice had increased levels of osteopontin in BALF following exposure to CeO_2. However, B6.Cg-*Kit*$^{W\text{-}sh}$ mice, which did not develop pulmonary inflammation in response to CeO_2, did not have increased osteopontin in lung tissue or BALF. A similar trend for an increase in osteopontin was observed in the hearts of CeO_2 instilled C57BL/6. Osteopontin is reported to play a role in the pathogenesis of inflammatory and immune-mediated diseases (Wang and Denhardt 2008) and more recently has been identified as a novel mast cell mediator which is produced by mast cells (Bulfone-Paus and Paus 2008; Nagasaka et al. 2008). Serum osteopontin levels are proposed as a biomarker for pneumoconiosis since an increase in osteopontin has been observed in asbestosis patients compared to healthy controls (Park et al. 2009). Osteopontin may influence the inflammatory response to particle exposure through increased recruitment of inflammatory cells such as eosinophils or potentially via increased phagocytosis of the particles (Pedraza et al. 2008; Takahashi et al. 2009). In support of this, it has been reported that osteopontin increases phagocytosis by macrophages (Schack et al. 2009). In addition, osteopontin induces airway remodeling and potentiation of pulmonary fibrosis by promoting differentiation of fibroblasts into myofibroblasts (Kohan et al. 2009). It remains to be determined if long-term CeO_2 exposure can result in pulmonary fibrosis through elevated osteopontin levels. In addition to effects on the pulmonary system, osteopontin is involved in cardiovascular remodeling and activation of vascular smooth muscle cells and therefore may represent a link between the pulmonary inflammation elicited by a nanoparticle and the subsequent adverse cardiovascular events (Okamoto 2007; Yin et al. 2009). In addition to osteopontin, we found an increase in TGF-β mRNA and protein in non-infarcted heart tissue from CeO_2 instilled C57BL/6 mice. Numerous studies have described a wide-spectrum of regulatory activities for TGF-β following cardiac infarction. TGF-β has been described as a protective mediator in models of myocardial ischemia/reperfusion and also participates in remodeling of heart tissue following injury by inducing the differentiation of fibroblasts to myofibroblasts as an example (Chen et al. 2003; Kossmehl et al. 2005). Our findings are similar to that observed in fine particulate matter exposed rats in which an increase in TGF-β was upregulated in heart tissue 24 h following particle exposure (Zhao et al. 2010). In our model, an upregulation of TGF-β in non-infarcted hearts following nanoparticle instillation may represent the induction of pathological processes such as tissue remodeling or may represent a protective mechanism to reduce systemic inflammation.

Previously, we demonstrated that ultrafine ambient particulate matter alters thoracic aorta reactivity 24 h following exposure (Cozzi et al. 2006). This is consistent with literature demonstrating an increase in vascular and myocardial complications within 24 h of exposure to increasing levels of ambient particulate matter and is the basis for why we measured

changes 24 h following instillation of CeO_2 (Brook et al. 2004; Roberts et al. 2007). In the present study we show that CeO_2 instillation impacts aortic vascular response to adenosine between the C57BL/6 and the B6.Cg-*Kit*$^{W\text{-}sh}$ mice differently (Figure 4). Additionally, there is a pattern of response that might suggest that a low dose of CeO_2 may potentiate a mast cell mediated relaxation signaling process (Figures 4 and 5). This result is interesting in light of a recent paper by Nui that found CeO_2 intravenous administration would protect against ischemic cardiomyopathy though an attenuation of oxidative stress or inflammatory processes that may be linked to the action of mast cells (Niu et al. 2007). Gojoiva and Kennedy reported that CeO_2 induces a small amount of inflammation in cultured endothelial cells with higher concentrations (Gojova et al. 2009; Kennedy et al. 2009). These studies were not thorough investigations of inflammatory pathway activation but they provide insight into how our model of exposure to CeO_2 might be exerting an effect on the vascular response probed by adenosine. Vascular dysfunction associated with particle exposure may be attributed to either a change in smooth muscle responsiveness or activation of the endothelium or both. This dysfunction may be attributed to an inflammatory response of pulmonary origin or the particle itself (Donaldson et al. 2005; Duffin et al. 2007). However, we did observe a more robust constrictor response at low concentrations of adenosine in the B6.Cg-*Kit*$^{W\text{-}sh}$ aortic rings when compared to the C57BL/6 aortic rings. This is interesting as mast cells are known to be residents of the wall adventitia of the vasculature and are recognized for their ability to release vasoactive mediators including histamine, chymase, adenosine, endothelin and lipoxygenase products (Dileepan and Stechschulte. 2006) which in turn can modulate vasoconstrictor activity in other vascular tissues (Doyle et al. 1994; Shepherd and Duling 1996; Shepherd et al. 1996).

At present, the data are most consistent with adenosine-receptor mediated dilation associated with CeO_2 that is mast cell dependent. Our results are the first to suggest a role for mast cells in adenosine-mediated vasoreactivity of the thoracic aorta following exposure to a particle. The recent work of Li et al. (2004) demonstrated that mast cell chymase can modulate blood pressure through an angiotensin II dependent mechanism; while work by Mackins reflects the cells impact on cardiac performance and norepinephrine release (Mackins et al. 2006). The latter report is relevant to our findings of I/R injury where we did not see expansion of the infarct in B6.Cg-*Kit*$^{W\text{-}sh}$ mice that was present in C57BL/6 mice following CeO_2 instillation. The overall significant difference in I/R injury between C57BL/6 and B6.Cg-*Kit*$^{W\text{-}sh}$ mice exposed to saline was not unexpected; rather it illustrates the role of mast cells in contributing to an ischemia-induced myocardial injury (Bhattacharya et al. 2007; Rork et al.2008). A hypothesis that adenosine may regulate vascular responsiveness and expansion of I/R injury through mast cells is supported by the finding that adenosine A2a receptor activation reduces myocardial infarct size by inhibition of resident mast cell degranulation (Rork et al. 2008). These data suggest that mast cells in cardiac and vascular tissues may play an influential role in response to an inflammatory process following a particle pulmonary challenge predisposing the cardiovascular system to adverse outcomes.

In total, the data presented demonstrate that CeO_2 can induce mast cell activation leading to the production of pro-inflammatory mediators. Through this process, the mast cell appears to have a significant role in recruitment of inflammatory cells leading to pulmonary inflammation. Subsequent to this pulmonary inflammatory process lung resident mast cells may release circulating factors that in turn activate mast cells and/or other immune cells in non-pulmonary tissues thereby amplifying the response systemically. Thus, mast cells appear to mediate an alteration in vascular responses and myocardial I/R injury in response to CeO_2 exposure. Taken together, these data provide evidence that CeO_2 can elicit an inflammatory response *in vivo* that is largely dependent upon mast cell activation thereby suggesting that mast cells should be explored as an important cell target of CeO_2 and possibly other-nanoparticle-induced inflammatory conditions.

References

Bhattacharya K, Farwell K, Huang M, Kempuraj D, Donelan J, Papaliodis D, Vasiadi M, Theoharides TC. Mast cell deficient W/Wv mice have lower serum IL-6 and less cardiac tissue necrosis than their normal littermates following myocardial ischemia-reperfusion. Int J Immunopathol Pharmacol. 2007; 20:69–74. [PubMed: 17346429]

Brook RD, Franklin B, Cascio W, Hong Y, Howard G, Lipsett M, Luepker R, Mittleman M, Samet J, Smith SC Jr, Tager I. Air pollution and cardiovascular disease: A statement for health-care professionals from the Expert Panel on Population and Prevention Science of the American Heart Association. Circulation. 2004; 109:2655–2671. [PubMed: 15173049]

Brown JM, Swindle EJ, Kushnir-Sukhov NM, Holian A, Metcalfe DD. Silica-directed mast cell activation is enhanced by scavenger receptors. Am J Respir Cell Mol Biol. 2007; 36:43–52. [PubMed: 16902192]

Brown JM, Wilson TM, Metcalfe DD. The mast cell and allergic diseases: Role in pathogenesis and implications for therapy. Clin Exp Allergy. 2008; 38:4–18. [PubMed: 18031566]

Bulfone-Paus S, Paus R. Osteopontin as a new player in mast cell biology. Eur J Immunol. 2008; 38:338–341. [PubMed: 18228246]

Chen H, Li D, Saldeen T, Mehta JL. TGF-beta 1 attenuates myocardial ischemia-reperfusion injury via inhibition of upregulation of MMP-1. Am J Physiol Heart Circ Physiol. 2003; 284:H1612–1617. [PubMed: 12679326]

Colon J, Herrera L, Smith J, Patil S, Komanski C, Kupelian P, Seal S, Jenkins DW, Baker CH. Protection from radiation-induced pneumonitis using cerium oxide nanoparticles. Nanomedicine. 2009; 5:225–231. [PubMed: 19285453]

Cozzi E, Hazarika S, Stallings HW 3rd, Cascio WE, Devlin RB, Lust RM, Wingard CJ, Van Scott MR. Ultrafine particulate matter exposure augments ischemia-reperfusion injury in mice. Am J Physiol Heart Circ Physiol. 2006; 291:H894–903. [PubMed: 16582015]

Dileepan KN, Stechschulte DJ. Endothelial cell activation by mast cell mediators. Methods Mol Biol. 2006; 315:275–294. [PubMed: 16110164]

Donaldson K, Mills N, MacNee W, Robinson S, Newby D. Role of inflammation in cardiopulmonary health effects of PM. Toxicol Appl Pharmacol. 2005; 207:483–488. [PubMed: 15979665]

Doyle MP, Linden J, Duling BR. Nucleoside-induced arteriolar constriction: A mast cell-dependent response. Am J Physiol. 1994; 266:H2042–2050. [PubMed: 8203602]

Duffin R, Mills NL, Donaldson K. Nanoparticles-a thoracic toxicology perspective. Yonsei Med J. 2007; 48:561–572. [PubMed: 17722227]

Gojova A, Lee JT, Jung HS, Guo B, Barakat AI, Kennedy IM. Effect of cerium oxide nanoparticles on inflammation in vascular endothelial cells. Inhal Toxicol. 2009; 21 (Suppl 1):123–130. [PubMed: 19558244]

Grimbaldeston MA, Chen CC, Piliponsky AM, Tsai M, Tam SY, Galli SJ. Mast cell-deficient W-sash c-kit mutant Kit W-sh/W-sh mice as a model for investigating mast cell biology in vivo. Am J Pathol. 2005; 167:835–848. [PubMed: 16127161]

Health Effects Institute. Evaluation of Human Health Risk from Cerium Added to Diesel Fuel. Vol. 9. 2001. Communication.

Kennedy IM, Wilson D, Barakat AI. Uptake and inflammatory effects of nanoparticles in a human vascular endothelial cell line. Res Rep Health Eff Inst. 2009:3–32. [PubMed: 19552347]

Kohan M, Breuer R, Berkman N. Osteopontin induces airway remodeling and lung fibroblast activation in a murine model of asthma. Am J Respir Cell Mol Biol. 2009; 41:290–296. [PubMed: 19151319]

Kossmehl P, Schonberger J, Shakibaei M, Faramarzi S, Kurth E, Habighorst B, von Bauer R, Wehland M, Kreutz R, Infanger M, Schulze-Tanzil G, Paul M, Grimm D. Increase of fibronectin and osteopontin in porcine hearts following ischemia and reperfusion. J Mol Med. 2005; 41(3):290–296.

Lin S, Reppert J, Hu Q, Hudson JS, Reid ML, Ratnikova TA, Rao AM, Luo H, Ke PC. Uptake, translocation, and transmission of carbon nanomaterials in rice plants. Small. 2009; 5:1128–1132. [PubMed: 19235197]

Lin W, Huang YW, Zhou XD, Ma Y. Toxicity of cerium oxide nanoparticles in human lung cancer cells. Int J Toxicol. 2006; 25:451–457. [PubMed: 17132603]

Mackins CJ, Kano S, Seyedi N, Schafer U, Reid AC, Machida T, Silver RB, Levi R. Cardiac mast cell-derived renin promotes local angiotensin formation, norepinephrine release, and arrhythmias in ischemia/reperfusion. J Clin Invest. 2006; 116:1063–1070. [PubMed: 16585966]

Nagasaka A, Matsue H, Matsushima H, Aoki R, Nakamura Y, Kambe N, Kon S, Uede T, Shimada S. Osteopontin is produced by mast cells and affects IgE-mediated degranulation and migration of mast cells. Eur J Immunol. 2008; 38:489–499. [PubMed: 18200503]

Niu J, Azfer A, Rogers LM, Wang X, Kolattukudy PE. Cardioprotective effects of cerium oxide nanoparticles in a transgenic murine model of cardiomyopathy. Cardiovasc Res. 2007; 73:549–559. [PubMed: 17207782]

Okamoto H. Osteopontin and cardiovascular system. Mol Cell Biochem. 2007; 300:1–7. [PubMed: 17136480]

Park B, Donaldson K, Duffin R, Tran L, Kelly F, Mudway I, Morin JP, Guest R, Jenkinson P, Samaras Z, Giannouli M, Kouridis H, Martin P. Hazard and risk assessment of a nanoparticulate cerium oxide-based diesel fuel additive – a case study. Inhal Toxicol. 2008a; 20:547–566. [PubMed: 18444008]

Park B, Martin P, Harris C, Guest R, Whittingham A, Jenkinson P, Handley J. Initial in vitro screening approach to investigate the potential health and environmental hazards of Enviroxtrade mark – a nanoparticulate cerium oxide diesel fuel additive. Part Fibre Toxicol. 2007; 4:12. [PubMed: 18053256]

Park EJ, Choi J, Park YK, Park K. Oxidative stress induced by cerium oxide nanoparticles in cultured BEAS-2B cells. Toxicology. 2008b; 245:90–100. [PubMed: 18243471]

Park EK, Thomas PS, Johnson AR, Yates DH. Osteopontin levels in an asbestos-exposed population. Clin Cancer Res. 2009; 15:1362–1366. [PubMed: 19174489]

Pedraza CE, Nikolcheva LG, Kaartinen MT, Barralet JE, McKee MD. Osteopontin functions as an opsonin and facilitates phagocytosis by macrophages of hydroxyapatite-coated microspheres: implications for bone wound healing. Bone. 2008; 43:708–716. [PubMed: 18656563]

Rao GV, Tinkle S, Weissman DN, Antonini JM, Kashon ML, Salmen R, Battelli LA, Willard PA, Hoover MD, Hubbs AF. Efficacy of a technique for exposing the mouse lung to particles aspirated from the pharynx. J Toxicol Environ Health A. 2003; 66:1441–1452. [PubMed: 12857634]

Roberts AP, Mount AS, Seda B, Souther J, Qiao R, Lin S, Ke PC, Rao AM, Klaine SJ. In vivo biomodification of lipid-coated carbon nanotubes by Daphnia magna. Environ Sci Technol. 2007; 41:3025–3029. [PubMed: 17533874]

Rork TH, Wallace KL, Kennedy DP, Marshall MA, Lankford AR, Linden J. Adenosine A2A receptor activation reduces infarct size in the isolated, perfused mouse heart by inhibiting resident cardiac mast cell degranulation. Am J Physiol Heart Circ Physiol. 2008; 295:H1825–1833. [PubMed: 18757481]

Schack L, Stapulionis R, Christensen B, Kofod-Olsen E, Skov Sorensen UB, Vorup-Jensen T, Sorensen ES, Hollsberg P. Osteopontin enhances phagocytosis through a novel osteopontin receptor, the alphaXbeta2 integrin. J Immunol. 2009; 182:6943–6950. [PubMed: 19454691]

Shepherd RK, Duling BR. Inosine-induced vasoconstriction is mediated by histamine and thromboxane derived from mast cells. Am J Physiol. 1996; 270:H560–566. [PubMed: 8779831]

Shepherd RK, Linden J, Duling BR. Adenosine-induced vasoconstriction in vivo. Role of the mast cell and A3 adenosine receptor. Circ Res. 1996; 78:627–634. [PubMed: 8635220]

Spanier JE, Robinson RD, Zhang F, Chan S, Herman IP. Size-dependent properties of CeO2-ψ nanoparticles as studies by Raman scattering. Physical Rev B. 2001:64.

Takahashi A, Kurokawa M, Konno S, Ito K, Kon S, Ashino S, Nishimura T, Uede T, Hizawa N, Huang SK, Nishimura M. Osteopontin is involved in migration of eosinophils in asthma. Clin Exp Allergy. 2009; 39:3323–3330.

Thill A, Zeyons O, Spalla O, Chauvat F, Rose J, Auffan M, Flank AM. Cytotoxicity of CeO2 nanoparticles for Escherichia coli. Physico-chemical insight of the cytotoxicity mechanism. Environ Sci Technol. 2006; 40:6151–6156. [PubMed: 17051814]

Walczak-Drzewiecka A, Wyczolkowska J, Dastych J. Environmentally relevant metal and transition metal ions enhance Fc epsilon RI-mediated mast cell activation. Environ Health Perspect. 2003; 111:708–713. [PubMed: 12727598]

Wang KX, Denhardt DT. Osteopontin: Role in immune regulation and stress responses. Cytokine Growth Factor Rev. 2008; 19:333–345. [PubMed: 18952487]

Wolters PJ, Mallen-St Clair J, Lewis CC, Villalta SA, Baluk P, Erle DJ, Caughey GH. Tissue-selective mast cell reconstitution and differential lung gene expression in mast cell-deficient Kit(W-sh)/Kit(W-sh) sash mice. Clin Exp Allergy. 2005; 35:82–88. [PubMed: 15649271]

Xia T, Kovochich M, Liong M, Madler L, Gilbert B, Shi H, Yeh JI, Zink JI, Nel AE. Comparison of the mechanism of toxicity of zinc oxide and cerium oxide nanoparticles based on dissolution and oxidative stress properties. ACS Nano. 2008; 2:2121–2134. [PubMed: 19206459]

Yin BL, Hao H, Wang YY, Jiang YJ, Xue S. Downregulating osteopontin reduces angiotensin II-induced inflammatory activation in vascular smooth muscle cells. Inflamm Res. 2009; 58:67–73. [PubMed: 19184356]

Zhao J, Xie Y, Qian X, Jiang R, Song W. Acute effects of fine particles on cardiovascular system: Differences between the spontaneously hypertensive rats and wistar kyoto rats. Toxicol Lett. 2010; 193:50–60. [PubMed: 20025942]

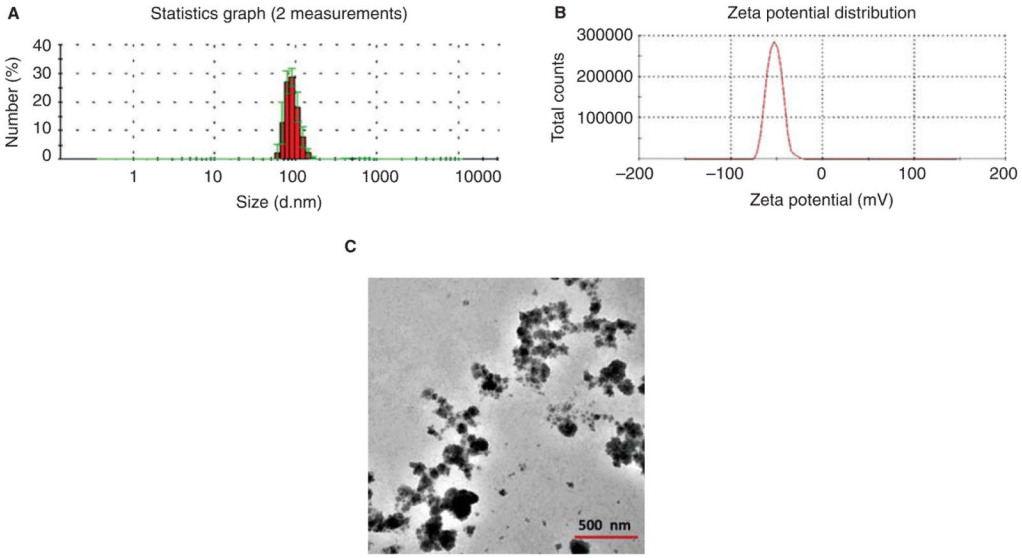

Figure 1.

Characterization of CeO_2 nanoparticles. (A) Hydrodynamic size distribution of CeO_2 suspension obtained by two independent measurements, showing an average size of 90 ± 20 nm (shown in red). The standard deviations are shown in green. (B) Zeta potential of CeO_2 suspension, indicating an average value of −52.7 mV. (C) TEM image of dehydrated CeO_2 suspension. A solution of 1 μg/μl CeO_2 was used for characterization.

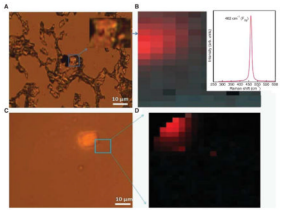

Figure 2.

Raman spectroscopy of CeO_2 nanoparticles in mouse lung tissue. (A) An optical image of a CeO_2-instilled C57BL/6 mouse lung section showing black colored CeO_2 at the surface. (B) The corresponding Raman image of the mouse lung section shown in (A). The red colored region is a map of the characteristic Raman peak (shown in the inset ~ 464 cm^{-1}) for CeO_2 nanoparticles. (C) Optical image of CeO_2 instilled mouse lung section showing CeO_2 embedded at ~ 4 μm depth. (D) The corresponding Raman map of the 464 cm^{-1} peak for the section shown in (C).

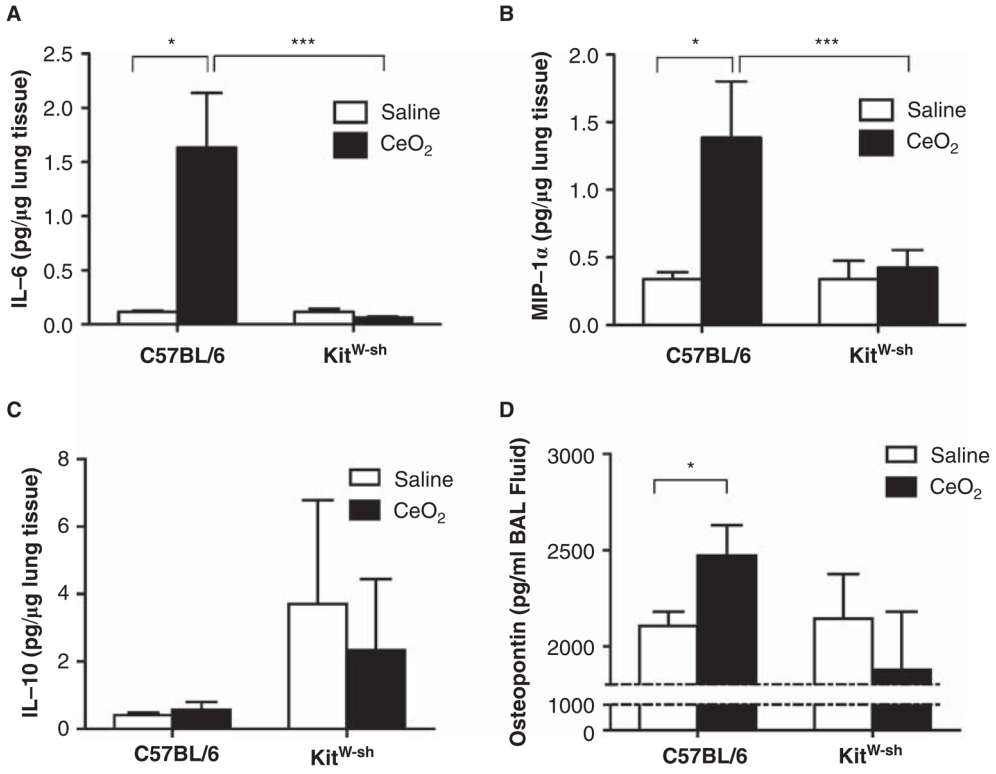

Figure 3.

Expression of inflammatory mediators in lung tissue and BALF in C57BL/6 and B6.Cg-*Kit*$^{W\text{-}sh}$ mice 24 hours after instillation of 100 μg CeO_2. (A) IL-6, (B) MIP-1α, (C) IL-10 protein levels measured in lung tissue 24 h following instillation of CeO_2 in C57BL/6 and B6.Cg-*Kit*$^{W\text{-}sh}$ mice. (D) Osteopontin protein levels measured in BALF of saline or CeO_2 instilled C57BL/6 and B6.Cg-*Kit*$^{W\text{-}sh}$ mice. n = 7–9 mice/group. ★$p \leq 0.05$.

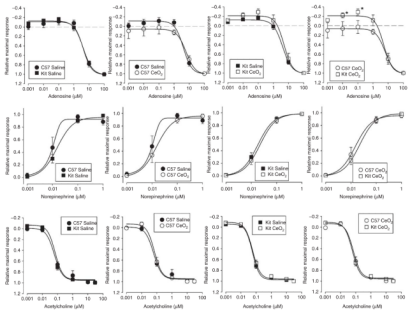

Figure 4.

Effect of CeO_2 instillation on the contraction and relaxation of isolated thoracic aorta from C57BL/6 or B6.Cg-*Kit*$^{W\text{-}sh}$ mice. (A) Adenosine concentration response profiles; (B) norepinephrine concentration response profiles and (C) acetylcholine concentration response profiles. Aortic rings were prestimulated with 1 μM phenylephrine. n = 6–10 mice/group. ★$p \leq 0.05$ versus C57BL/6.

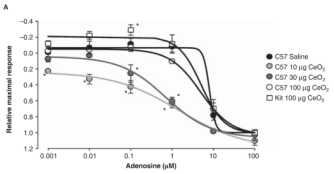

Figure 5.

Comparison of the adenosine dose-response of thoracic aortic ring segments from C57BL/6 mice exposed to 10, 30 and 100 μg of CeO_2 and B6.Cg-*Kit*$^{W\text{-}sh}$ mice exposed to 100 μg of CeO_2. n = 6–10 mice/group. ★$p \leq 0.05$ as compared to saline treated mice.

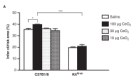

Figure 6.

Comparison of the size of myocardial infarction in C57BL/6 exposed to 10, 30 and 100 μg of CeO_2 and B6.Cg-*Kit*$^{W\text{-}sh}$ mice exposed to 100 μg of CeO_2. Twenty-four hours after instillation with either saline or CeO_2, the LAD was ligated for 20 min and then reperfused for 2 h. n = 3–4 mice/group. ★$p \leq 0.05$ ★★★ $p \leq 0.001$.

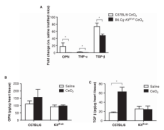

Figure 7.

Expression of osteopontin, TNF-α and TGF-β in non-infarcted heart tissue following CeO_2 instillation. (A) mRNA levels of osteopontin, TNF-α and TGF-β in non-infarcted heart tissue following CeO_2 instillation in C57BL/6 or B6.Cg-*Kit*$^{W\text{-}sh}$ mice. (B) Osteopontin and (C) TGF-β protein levels in non-infarcted heart tissue following CeO_2 instillation in C57BL/6 or B6.Cg-*Kit*$^{W\text{-}sh}$ mice. n = 3–4 mice/group. ★$p \leq 0.05$.

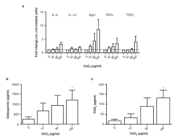

Figure 8.

Effect of CeO_2 on *in vitro* BMMC activation. (A) Fold change in mRNA expression of IL-6, IL-13, osteopontin (Spp1), TNF-α and TGF-β 2 hours following CeO_2 treatment of BMMCs as compared to untreated cells. (B) Osteopontin protein levels measured in the supernatant of BMMCs exposed to CeO_2 for 24 h as measured by ELISA. (C) PGD_2 levels measured in supernatant of BMMCs exposed to CeO_2 for 1 h as measured by EIA. n = 3–5 independent experiments. $^{\star}p \leq 0.05$.

Table I

Effect of CeO_2 on bronchoalveolar lavage (BAL) cell populations.

Strain	Treatment	Total cells ($\times 10^3$)	Macrophages ($\times 10^3$)	Epithelial cells ($\times 10^3$)	Neutrophils ($\times 10^3$)	Eosinophils ($\times 10^3$)	Lymphocytes ($\times 10^3$)
C57BL/6	Saline	39.6 ± 1.7	35.0 ± 1.7	4.0 ± 1.3	0.4 ± 0.3	0.1 ± 0.1	0.5 ± 0.2
C57BL/6	10 μg CeO_2	27.3 ± 7.1	21 ± 8.6	2.5 ± 4.7	2.4 ± 1.3★	0.2 ± 0.1	1.2 ± 0.7
C57BL/6	30 μg CeO_2	23 ± 5.7	17 ± 2.5	2.3 ± 1.4	2.3 ± 1.2★	0.5 ± 0.4	2.0 ± 0.9★
C57BL/6	100 μg CeO_2	91.5 ± 8.9★	81.1 ± 8.2★	5.8 ± 0.9	3.3 ± 1.0★	0.1 ± 0.1	1.3 ± 0.2★
B6.Cg-*Kit*$^{W\text{-}sh}$	Saline	48.9 ± 5.0	42.5 ± 5.4	4.9 ± 1.1	0.4 ± 0.1	0.2 ± 0.2	0.9 ± 0.2
B6.Cg-*Kit*$^{W\text{-}sh}$	100 μg CeO_2	61.8 ± 5.7†	53.0 ± 5.3†	6.3 ± 2.5	1.8 ± 1.0	0.0 ± 0.0	0.7 ± 0.3

Values are mean ± SEM. n = 5–10/group.

★ $p < 0.05$ vs saline within strain.

† $p < 0.05$ vs C57BL/6 within treatment.

Table II

Calculated mean EC_{50} values based on cumulative addition concentration-response profiles of thoracic aortic rings from C57BL/6 and B6.Cg-*Kit*$^{W\text{-}sh}$ mice.

Treatment	Endothelium	C57BL/6 saline	C57BL/6 10 μg CeO_2	C57BL/6 30 μg CeO_2	C57BL/6 100 μg CeO_2	B6.Cg-*Kit*$^{W\text{-}sh}$ saline	B6.Cg-*Kit*$^{W\text{-}sh}$ 100 μg CeO_2
Adenosine	Denuded	7.52 ± 1.29 μM	4.74 ± 1.83 μM	4.87 ± 1.25 μM	5.61 ± 1.08 μM	4.65 ± 0.97 μM	4.76 ± 1.35 μM
Norepinephrine	Intact	26.31± 2.31 nM	11.31 ± 5.71 nM	17.18 ± 3.38 nM	27.01 ± 8.17 nM	30.21 ± 3.21 nM	32.52 ± 3.15 nM
Acetylcholine	Intact	79.88 ± 17.25 nM	93.24 ± 7.84 nM	76.23 ± 12.00 nM	84.79 ± 14.58 nM	71.54 ± 20.01 nM	75.46 ± 19.22 nM
Sodium nitroprusside	Denuded	4.35 ± 0.90 nM	1.25 ± 0.03 nM	2.19 ± 1.07 nM	3.63 ± 1.36 nM	5.16 ± 1.11 nM	4.23 ± 1.04 nM

Values are mean ± SEM. n = 4–10/group.